Electron Densities of Three B_{12} Vitamins

Stefan Mebs,[†] Julian Henn,[‡] Birger Dittrich,[‡] Carsten Paulmann,[§] and Peter Luger*,[†]

Institut für Chemie und Biochemie/Kristallographie, Freie Universität Berlin, Fabeckstrasse 36a, 14195 Berlin, Germany, Institut für Anorganische Chemie, Georg-August-Universität Göttingen, Tammannstrasse 4, 37077 Göttingen, Germany, Mineralogisch-Petrographisches Institut, Universität Hamburg, Grindelallee 48, 20146 Hamburg, Germany

Received: March 18, 2009; Revised Manuscript Received: May 18, 2009

The electron densities of the three natural B_{12}-vitamins, two of them being essential cofactors for animal life, were determined in a procedure combining high-order X-ray data collection at low to very low temperatures with high-level density functional calculations. In a series of extensive experimental attempts, a high-order data set of adenosylcobalamin (AdoCbl) could be collected to a resolution of sin $\theta/\lambda = 1.00$ Å^{-1} at 25 K. This modification contains only minor disorder at the solvent bulk. For methylcobalamin (MeCbl), only a severely disordered modification was found (sin $\theta/\lambda = 1.00$ Å^{-1}, 100 K, measured with synchrotron radiation). The already published data set of cyanocobalamin (CNCbl) (sin $\theta/\lambda = 1.25$ Å^{-1}, 100 K) was reintegrated to guarantee similar treatment of the three compounds and cut to sin $\theta/\lambda = 1.11$ Å^{-1} to obtain a higher degree of completeness and redundancy. On the basis of these accurate experimental geometries of AdoCbl, MeCbl, and CNCbl, state-of-the-art density functional calculations, single-point calculations, and geometry optimizations were performed on model compounds at the BP86/TZVP level of theory to evaluate the electronic differences of the three compounds. AdoCbl and MeCbl are known to undergo different reaction paths in the body. Thus, the focus was directed toward the characterization of the dative Co−C_{ax} and Co−N_{ax} bonds, which were quantifed by topological parameters, including energy densities; the source function including local source; and the electron localizability indicator (ELI-D), respectively. The source function reveals the existence of delocalized interactions between the corrin macrocycle and the axial ligands. The ELI-D indicates unsaturated Co−C_{ax} bonding basins for the two biochemically active cofactors, but not for CNCbl, where a population of 2.2*e* is found. This may be related to significant π-backbonding, which is supported by the delocalization index, δ, of 0.15 between the Co atom and the N atom of the cyano ligand. Considering all results, the inherent electronic differences between AdoCbl and MeCbl are found to be small thus, supporting earlier findings that the interaction with the protein site mainly controls the type of Co−C_{ax} bond cleavage.

Introduction

Since their discovery, the B_{12}-Vitamins (cobalamines, Cbl's) have remained a focus of science, since they serve as cofactors in several enzyme systems and belong to the most complex nonpolymeric structures in nature. Furthermore, Hodgkin and co-workers discovered in 1961[1] that they carry a cobalt−carbon bond, which is unique in nature. The general structure is given in Figure 1. All derivatives have in common the partially unsaturated corrin macrocycle substituted with seven amide chains. One of them is connected to the Co center at the α-position below the ring via the so-called nucleotide loop. The β-position is occupied by a cyano ligand in cyanocobalamin (CNCbl), methyl in methylcobalamin (MeCbl), and 5′-deoxyadenosyl in adenosylcobalamin (AdoCbl). This particular Co−C_{ax} bond is of special interest, because it mainly undergoes ionic cleavage in MeCbl[2] and always radical cleavage in AdoCbl,[3] which are the two biologically active derivatives of this class of compounds. CNCbl, vitamin B_{12} itself, is a product of extraction and biochemically inert, because the cyano ligand is a strong σ-donor as well as weak π-acceptor. Due to the different in vivo reaction behavior of these essential molecules, an analysis of the electronic differences of the Co−C_{ax} bond is highly desirable, which is carried out in this work with combined state-of-the-art experimental and theoretical electron density methods.

All three substances are diamagnetic,[4] and cobalt is assumed to be formally in the Co^{III} oxidation state within a low-spin-configured, slightly distorted, octahedral ligand field. In contrast to the highly conjugated porphyrin ring (18 π-electrons distributed over 18 atoms), the corrin macrocycle exhibits more conformational freedom (14 π-electrons distributed over 13 atoms). Due to this and because the 5,6-dimethylbenzimidazole group (DMB) is replaced by a histidine (His) ligand from the protein in some enzymes (see ref 5 and references therein), concepts for Co−C_{ax} bond activation have been developed which include a stereoelectronic trans-axial effect (α to β) connected with butterfly bending of the corrin ring toward the β-ligand.[6] However, in later studies,[7,8] these concepts have largely been ruled out. In addition, replacing DMB with a water molecule has minor effects on the Co−C_{ax} bond.[9] As long as the β-ligand is the stronger σ-donor, this ligand dominates the electronic properties of both the Co−C_{ax} and the Co−N_{ax} bond. Thus, an inverse trans-axial effect is operative.[10]

A wide range of experimental and theoretical studies were published in this field in the past decade.[11−42] A spectroscopic

* Corresponding author. E-mail: luger@chemie.fu-berlin.de.
[†] Freie Universität Berlin.
[‡] Georg-August-Universität Göttingen.
[§] Universität Hamburg.

10.1021/jp902433x CCC: $40.75
Published on Web 07/01/2009

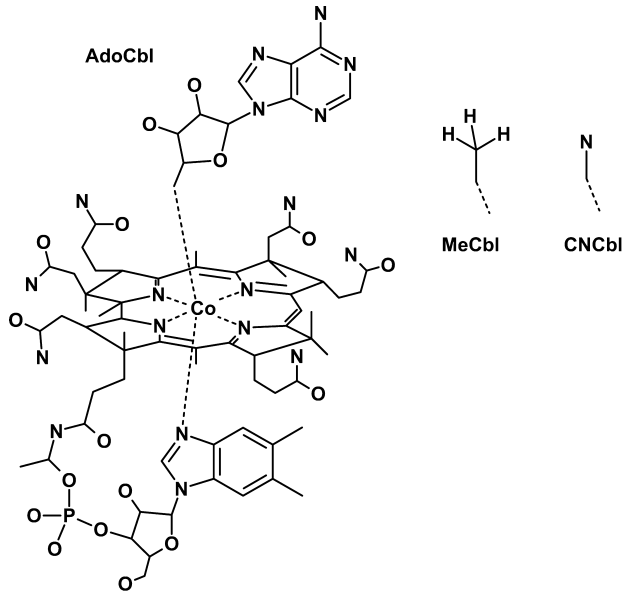

Figure 1. Structures of the two native B_{12} cofactors (adenosylcobalamin (AdoCbl) and methylcobalamin (MeCbl), respectively), which are biologically active, and cyanocobalamin (CNCbl), which is a product of extraction (known as vitamin B_{12}).

study of 2003 focused on the detailed description of the electronic differences of the isolated molecules.[9] With experimental (Abs and (M)CD) and computational methods, they obtained insight into the molecular orbitals (MO) scheme that differs essentially between H_2OCbl^+ and CNCBl on one hand and MeCbl and AdoCbl on the other hand. However, since the Abs and (M)CD spectra of the alkyl derivatives (AdoCbl and MeCbl) are almost identical, the inherent electronic differences of these two compounds could not be assigned completely. The final suggestion of the authors was that the $Co-C_{ax}$ bond activation through interaction with the protein side plays the major role for the different reaction paths. This is supported by the fact that the homolysis rate of AdoCbl is about 10−12 magnitudes lower for AdoCbl when it is solved in water, as compared to the activity in its corresponding protein.[43] In addition, the partial density-of-state analysis of the three compounds showed no significant difference between MeCbl and AdoCbl.[36] A recent study by Jensen and Ryde[10] revealed in detail how the $Co-C_{ax}$ bond is weakened through interaction with the protein so that both biochemical reactivity and inherent electronic differences of the three cobalamines are largely understood. However, electron density (ED) determinations of systems of this size are a meaningfull test case for the experimental limits in obtaining suitable data sets as well as for the explanatory power of properties derived from the ED.

Experimental electron density studies of transition metal complexes have been performed since the early 1970s[44] but, of course, in a more qualitative fashion at that time. Due to the enormous progress in hardware (synchrotron radiation, CCD detectors, computer power) and software, the number of publications has increased considerably up to now.[45] At the same time, the programs for theoretical quantum chemical calculations have developed dramatically, and new partitioning and interpretation schemes such as the quantum theory of atoms in molecules (AIM)[46] and the natural bond orbitals (NBO)[47] have emerged so that quantitative description of electron densities in transition metal complexes approach being a routine application nowadays.

In addition to metallocarbonyls and other small compounds, a series of metalloporphyrins and -phtalocyanins were carefully investigated in the 1980s.[48−55] The more complex cobalamin systems were unachievable at that time, because area detection was not developed yet, so it took until 2007 for the first electron density study of cyanocobalamin to appear.[56] Nowadays, new tools, such as the source function (SF),[57,58] and the electron localizability indicator (ELI-D),[59] which promise deeper understanding of chemical interactions, are available. The SF displays the amount of electron density provided by each atom to any reference point, which means also for atoms which are not directly connected to the reference point. In such a way, delocalization effects can be manifested on absolute numbers. This is also possible with the delocalization index, δ, introduced by Bader and Stephens,[60,61] The ELI-D is a further development of the ELF.[62,63] These concepts divide space into regions of localized electrons instead of atoms and therefore greatly complement the AIM theory. The partitioning follows the same rules that are used by AIM to separate atoms from each other.[46] Thus, it is space-filling and discrete, providing reliable integrated electron numbers of both core shells and (non)bonded valence electrons. The disadvantage of the ELF, not to be comparable between different molecules because the localization is always related to a uniform electron gas of the same compound, was discarded with the introduction of the ELI-D.

It has been known since the early days of multipole modeling[64] that the restriction to single-ζ Slater radial functions causes systematic shifts of the ED-derived properties in all compounds, including higher elements. On a smaller scale, this effect is also visible in bonds between light atoms (C, N, O), a topic which was extensively discussed some years ago.[65−68] In TM-C (TM = transition metal) bonds, the ED at the bond critical point (bcp) is very low, whereas the bond-parallel curvature, λ_3, is very high so that the effect of the radial functions is pronounced. Recent developments employ double- or triple-ζ functions by projection of Stockholder pseudoatoms into nucleus-centered spherical harmonics.[69] However, since these developments are yet not implemented in the available software and the discussion of this study is focused on the topological differences between the Cbl's rather than on absolute numbers, the standard model, which was extensively used for the last 30 years to describe TM-complexes, must be appropriate; but to account for this problem as much as possible, bond topological descriptors are compared to values from theory.

Experiments and Refinement Procedures

The experimental procedures concerning CNCbl are given in reference 56. Single crystals of AdoCbl and MeCbl were obtained by slow gas diffusion of acetone, ethanol, or isopropyl alcohol into saturated aqueous solutions of the Cbl's. All three compounds produce optically perfect dark red crystals of remarkable size up to 0.5 cm^3. Nevertheless, collecting X-ray data of Cbl crystals suitable for electron density determination is far from trivial. There are two major problems for these substances: crystal instability and disorder. Once crystals of CNCbl or MeCbl are taken out of the mother liquor, they decompose within seconds because they loose solvent. Hence, they have to be prepared and mounted under constant cooling. In contrast, AdoCbl yields crystals that are stable outside the liquor for at least some hours, but like CNCbl and MeCbl, they break very easily during the process of mounting and cooling, shock-cooling as well as slow-cooling. For CNCbl, a high-order X-ray data set (sin θ/λ = 1.25 $Å^{-1}$) could be obtained, which was published in 2007.[56]

To obtain electron density quality data for the other target molecules, nine high-order data sets of several modifications

TABLE 1: Crystallographic Data and Experimental Conditions for the Cobalamines

	compound		
	AdoCbl	MeCbl	CNCbl
empirical formular	$C_{72}H_{100}CoN_{18}O_{17}P \cdot 2C_2H_6O \cdot 11H_2O$	$C_{63}H_{91}CoN_{13}O_{14}P \cdot 21H_2O$	$C_{63}H_{88}CoN_{14}O_{14}P \cdot 3C_3H_8O \cdot 12H_2O$
formular weight (g/mol)	7472.63	7242.13	7007.39
crystal system	orthorhombic	orthorhombic	orthorhombic
space group (no.)	$P2_12_12_1$ (19)	$P2_12_12_1$ (19)	$P2_12_12_1$ (19)
Z	4	4	4
temp (K)	25	100	100
space group	$P2_12_12_1$	$P2_12_12_1$	$P2_12_12_1$
a (Å)	15.120(3)	17.293(3)	15.831(3)
b (Å)	21.474(4)	17.687(3)	22.374(4)
c (Å)	27.219(6)	32.218(6)	25.304(5)
V (Å^3)	8837.7(1)	9863.6(1)	8962.6(1)
calcd density (g/cm^3)	1.404	1.219	1.298
F(000)	3987	3824	3760
crystal form	block	block	block
crystal size (mm^3)	0.6 × 0.5 × 0.45	0.4 × 0.3 × 0.3	0.4 × 0.4 × 0.4
λ (Å)	Mo Kα, 0.7107	syn, 0.56	Mo Kα, 0.7107
sin θ/λ (Å^{-1})	1.00	1.00	1.11
collected reflections	663 077	556 782	545 036
symmetry independent	73 277	79 977	100 714
completeness (%)	98.5	96.8	98.1
redundancy	9.0	7.0	5.4
R_{int}	7.40	3.20	3.59
R_1 (spherical)	5.48	8.12	4.07
N_{ref}/N_{var} (multipole)	38.5		57.8
$R_w(F)$ (multipole)	4.47		3.33
$R(F)$ (multipole)	4.86		3.42
$R_{all}(F)$ (multipole)	6.31		7.01
included ($I > 3\sigma$)	63868		82288
GoF	2.92		2.62

(AdoCbl·acetone, AdoCbl·ethanol, AdoCbl·isopropyl alcohol, and MeCbl·water) were collected at five different experimental setups (beamlines F1 and D3 at HASYLAB, Hamburg, and three conventional setups, including our diffractometer with closed-cycle helium cryostat and a setup with rotating anode). Due to the fact that a perfect diffraction pattern can hide a severly disordered structure and that measurement periods are limited (especially at synchroton sources), only a limited number of attempts could be made to cool the crystals in a time range of several hours to reduce crystal decomposition and disorder. Moreover, slow cooling was just technically not possible at D3 and at one of the conventional setups. Unfortunately, it turned out that slow cooling is essential for AdoCbl and MeCbl, since only one data set (AdoCbl·ethanol) measured at our own diffractometer under slow cooling down to 25 K yielded a structure, which contains only minor disorder in parts of the solvent bulk. However, for CNCbl, shock-cooling to 100 K was successful.

For MeCbl, only a heavily disordered modification was found, see Figure 2. The earlier measured data set of CNCbl[56] was reintegrated to guarantee similar treatment for the two conventional measurements (CNCbl and AdoCbl). Furthermore, since the disorder was treated differently from before, the results for CNCbl are also included in Table 1, which lists details on the crystal data and the experimental conditions. An empirical absorption correction was applied ($\mu \approx 0.3$ mm^{-1}) for CNCbl and AdoCbl. Table 1 lists crystallographic and experimental details only of the three data sets that were further examined. The other (above-mentioned) data collections had to be discarded because of severe disorder problems.

Modeling of the aspherical electron density distributions was performed for CNCbl and AdoCbl with XD2006,[70] which employs the multipole formalism of Hansen and Coppens[71] and permits the calculation of new properties such as the source function.[57] The multipoles were expanded to the hexadecapole level for all non-hydrogen atoms, and the hydrogen atoms were represented by monopoles and bond-directed dipoles. The multipole populations of chemically equivalent atoms were constrained to each other, and local m-symmetry was applied to all planar fragments, such as amide residues and heterocycles, and to all sp^3-hybridized atoms with two equal atoms bonded to it. C_{3v} symmetry was imposed on the methyl groups. For the Co atom, the corrin ring, and both axial ligands, the expansion/contraction parameters κ and κ' were taken from refinements of theoretical structure factors of smaller model compounds gained from the experimental geometries (see the next section) and adjusted in the experimental refinements. Both free refinement and tetragonal symmetry 4 (only Y_{00}, Y_{40}, Y_{44+}, and Y_{44-} are refined) were tested as local symmetry for the Co atom. Since free refinement of the Co atom did not lead to significant changes, all derived properties were obtained from the models in which the Co atom has 4-fold symmetry. A perfect octahedral local symmetry would allow only two multipoles: the Y_{00} and the cubic harmonic $Y_{40} + 0.7403Y_{44+}$.[88] However, all investigated systems are slightly distorted and are of lower crystallographic symmmety, the separate refinement of Y_{40} and Y_{44+}, Y_{44-} is justified. The H atom positions were fixed to neutron distances.[72] Due to these restrictions, the reflex over parameter ratio exceeded 25 in all refinements. Because some of the monopole populations of the solvent atoms refined to physically unsound values, only conventional parameters were refined.

It is known[73,88] that the results of the fit for neutral atom scattering factors (Co) and its ionic counterparts (Co^{2+}, Co^{3+}, respectively) are virtually identical in experimental refinements. These valence states correspond to the following notation: (18 electrons core) $(3d)^x(4s^2)$ for Co and (18 electrons core) $(3d)^x$ for Co^{2+}/Co^{3+}, x being a least-squares variable. Due to the diffuse character of the 4s electrons, only a few low-order

reflections are influenced by them. This effect is enhanced in noncentrosymmetric space groups, where the structure factor phases are generally worse determined.[74] This is the case here: all modifications found for the Cbl's crystallize in $P2_12_12_1$. This means that asphericity is a much better defined property than net charge.[88] Within the refinements of the theoretical structure factors (see next section), the best fit was obtained for the neutral atomic scattering factors, with a fixed 4s population of two electrons. Therefore, it was decided to use the neutral scattering factors in the experimental refinements, as well. In several experimental studies,[75,76] the neutral scattering factors were favored, too.

Theoretical Calculations

Studies dealing with physical properties obtained by experiment generally justify their results by comparison with calculations, if possible. In ED publications, experimental results are compared to either single-point calculations or to results from optimized geometries, or if the systems are small enough, periodic calculations are performed. It is known for TM complexes that the optimized structures depend significantly on the applied method (e.g., HF, DFT, MP2) and on the flexibility of the basis set.[31] Therefore, many studies focused on this methodological aspect. The outcome is that there is no systematic correlation between compound class and method/basis set applied, so for each class of compounds, the optimal method and basis set has to be evaluated in a mainly empirical way. Due to the size of the examined molecules and the focus of this study, such comparison is far beyond possibility and scope.

Since up to now, available X-ray data of Cbl's[22−24] were of limited resolution, all theoretical studies had to rely on optimized geometries exclusively. Within this study, experimental geometries of high accuracy are at hand which may provide deeper insight into the intrinsic electronic differences among the three molecules. The experimentally determined structures of the three compounds (two of them obtained from preliminary multipole refinements (CNCbl and AdoCbl), the MeCbl structure from spherical refinement) were reduced to their essential parts (see also Figure 3). To get the best relation between reliable model and computer time, the total structure was reduced to only a minimal degree: all amide chains, the two methyl groups of DMB, and the nucleotide loop were removed, leaving only a methyl-substituted benzimidazole as an α axial ligand. Because the PO_4 group, which carries a negative charge, is absent in the models, they are assigned a charge of +1. Furthermore, the nucleoside was removed in the case of AdoCbl, leaving the ribose as the β-ligand. Although computer power has dramatically increased in the last several years, this reduction is still necessary because the calculations presented in this study are very time- and storage-demanding. Single-point calculations as well as geometry optimizations have been performed with the functional BP86[77] and the basis set TZVP of Ahlrichs[78] as implemented in Gaussian03.[79] Both the functional and the basis set have already been in use in earlier theoretical studies on Cbl's.[9] The other widely used functional, B3LYP, is known to systematically underestimate the bond dissociation energy of the $Co-C_{ax}$ bonds in this class of compounds[30] and was therefore not used here. Three programs were employed to obtain diverse ED-properties from the calculated models, at both experimentally derived and optimized geometry.

The program AIM2000[80] was used for calculating the bond topological properties of the six Co−X bonds, including the integrated number of electrons within the zero flux surfaces (ZFS). Furthermore, integrated atomic properties (AIM charges and volumes and delocalization index)[60] of Co and the six atoms coordinated to Co were obtained.

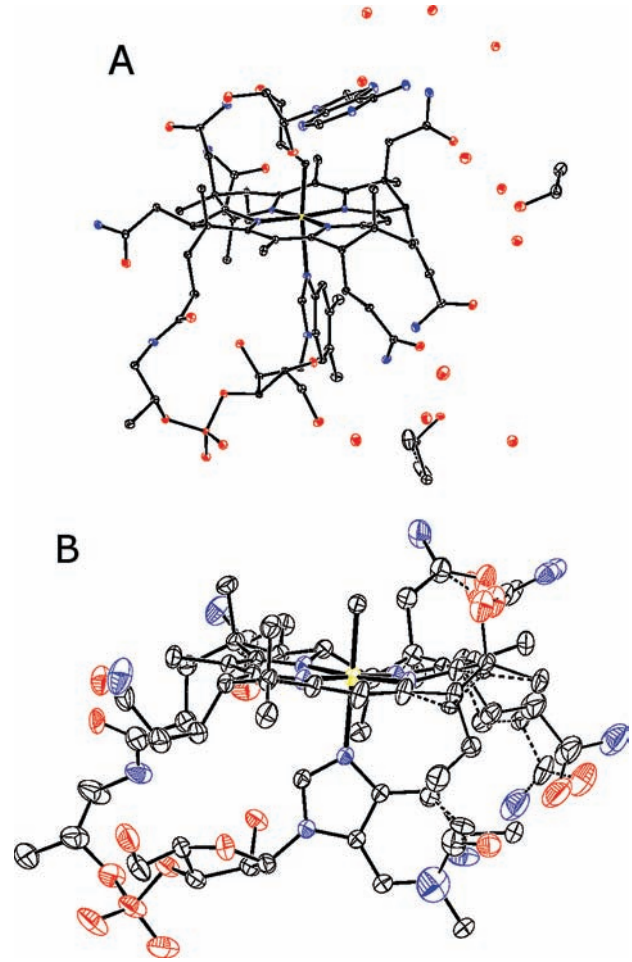

Figure 2. Experimental high-resolution structures of AdoCbl at 25 K (A) and MeCbl at 100 K (B). In the solvent bulk, only minor disorder is found at one ethanol and two water molecules in the case of AdoCbl. MeCbl shows severe disorder also at the corrin ring. For clarity, hydrogen atoms are not shown.

Additionally, theoretical structure factors were obtained with the program Tonto[81] (pseudo periodic calculations) using the checkpoint files obtained by Gaussian03. Subsequent XD-refinements were performed with the same local coordinate systems and symmetry restrictions as in the experimental cases. Additionally, the valence-deformation radial fits were optimized by refinement of the κ' parameters of all non-hydrogen pseudoatoms, which was not possible in the experimental case. Refinement of the deformation monopoles ($P_{lm\pm} = P_{00}$) did not lead to physically meaningful results for the theoretical models and was therefore not employed in the refinements.

Finally, the programs Dgrid4.3 and Basin4.3[82] were used for calculation of the electron localizability index (ELI-D) and the integrated atomic properties of the remaining atoms because it is not possible to integrate 80−100 atoms with AIM2000 in a reasonable amount of time. The grid size was 0.075 bohr. The core region of the Co atom was integrated with a grid size of 0.02 bohr for all Cbl's.

Results and Discussion

Structures. The structures of AdoCbl at 25 K and MeCbl at 100 K are displayed in Figure 2 as ORTEP representations.[83]

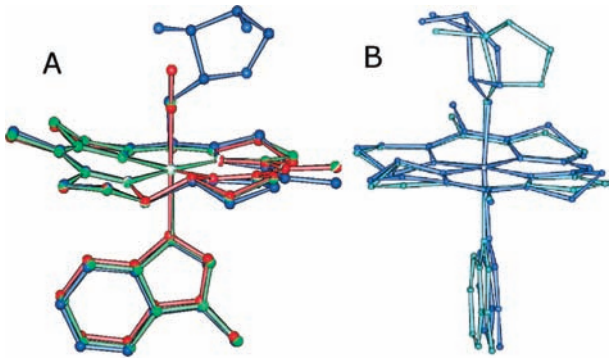

Figure 3. (A) Superposition of the three model compounds at experimental geometry. Red, CNCbl; green, MeCbl; and blue, AdoCbl. (B) Superposition of AdoCbl at experimental (blue) and optimized (light blue) geometry. Schakal representation.

For reasons of clarity, the numbering schemes and H atoms are excluded. For MeCbl, the large number of water molecules is also not shown. In AdoCbl (A), only minor disorder is present, which is located at one ethanol and two water molecules. In contrast, the solvent bulk in MeCbl (B) is heavily disordered; in addition, one-half of the corrin macrocycle shows disorder. The 100 K structure of CNCbl is not shown, because it is given in reference 56.

Figure 3A shows the superposition of the three model molecules (introduced in the previous section) from experimental coordinates as a Schakal representation:[84] CNCbl in red, MeCbl in green, AdoCbl in blue. It can easily be seen that the cyano ligand (CNCbl) as well as the corresponding axial N atom are closer to the Co center than the axial ligands in the alkylcobalamines. This is due to the already mentioned inverse trans-axial effect from the β- to the α-ligand. A further aspect is that the corrin-folding is slightly different in the case of AdoCbl at the side where the nonbonded electrons of the ribose oxygen interact stereoelectronically with the corrin ring. These effects are also found in the optimized geometries and are to be understood in terms of electron density analysis. The overall conformational changes after geometry optimization are small for CNCbl and MeCbl. Only AdoCbl shows a rotation of the β-ligand (see Figure 3 B; optimized geometry in light blue). In all cases, the distortion of the octahedral ligand field as well as the corrin fold decreased via optimization due to the absence of the amide chains.

Table 2 lists all bond lengths and angles of the distorted octahedral ligand sphere around the Co atom for the three compounds obtained from experiment and geometry optimization. The experimental data of CNCbl and AdoCbl are the results of multipole modeling, the MeCbl geometry is taken from the spherical refinement. For the disordered atom sites in the corrin ring of MeCbl, the major contributors (95%) were taken. The experimental values compare very well to those presented in ref 36. The $Co-N_{eq}$ (N_{eq} = N21−N24) bond distances vary around 0.02 Å within the three molecules, and all $N_{eq}-Co-N_{eq}$ and $N_{eq}-Co-N_{ax}$ angles are identical within 1.5 degrees. The two axial bonds show the expected inverse trans effect in the bond lengths. For the experimental cases, significant differences are found for some angles, including the axial carbon atom, mainly $N_{ax}-Co-C_{ax}$, which is expected because of the different sterical demands of the β-ligands. This effect disappears after geometry optimization because of the mentioned absence of amide chains. A small sterical effect of the β-ligand still remains. This can be deduced from the different amount of change in the angle N21−C1−C19−N24 between experimental and optimized geometry: CNCbl and MeCbl show a decrease of approximately 3.5 and 4.5 degrees, respectively, whereas AdoCbl shows a decrease of only about 1.5 degrees. As expected, the optimization elongates the $Co-N_{ax}$ bond significantly, but the $Co-C_{ax}$ bond is unaffected in the cases of MeCbl and AdoCbl. Furthermore, a systematic shift of the α-ligand is found: the N21−Co−N_{ax} and N24−Co−N_{ax} angles decrease in all three compounds, whereas the angles N22−Co−N_{ax} and N23−Co−N_{ax} increase upon optimization. It follows that the averaged deviation from 90 degrees is smaller for all four angles. In the case of AdoCbl, the same takes place for the β-ligand. The decreased distortion is also reflected in the $N_{ax}-Co-C_{ax}$ angle, which approaches significantly closer to 180° for all three Cbl's.

Bond Topology. Figure 4 displays the experimental static deformation density maps for CNCbl (A) and AdoCbl (B) in the plane of the corrin macrocycle. Both show the expected electron accumulations in the covalent bonds as well as the "key-lock arrangement" in the dative bonds to the Co center.

Table 3 lists the experimental bond descriptors of the $Co-C_{ax}$ and $Co-N_{eq/ax}$ (N_{eq} = N21, N22) bond critical points bcp of CNCbl and AdoCbl. The four $Co-N_{eq}$ bonds group into two pairs of bonds that are chemically almost identical, so only one is given for each. The shorter one will be denoted Co−N21; the longer, Co−N22, following the common nomenclature. In CNCbl, the bond lengths increase in the following order: $Co-C_{ax} < Co-N_{eq} < Co-N_{ax}$, accompanied by a decrease in the ρ value at the bcp. This order changes for AdoCbl, for which the $Co-C_{ax}$ bond is significantly longer and weaker. Due to the electronic inverse trans effect, the $Co-N_{ax}$ bond becomes longer and weaker, as well. Interestingly, the ρ values of the four $Co-N_{eq}$ bonds differ between CNCbl and AdoCbl, which may point toward an additional cis electronic effect of the β-ligand. However, this is not supported by theoretical results (see below). The Laplacian at the bcp of the $Co-C_{ax}$ bonds is less positive than for the $Co-N_{eq}$ bonds, although they have comparable distances in the case of CNCbl. The values are even lower than for the $Co-N_{ax}$ bonds, although they are ~0.2 Å longer. This points toward covalent contributions in the $Co-C_{ax}$ bonds. This is supported by the values for the total energy densities, obtained with Abramov's relation.[85] Since the experimental values depend on the refined model and Abramov's relation is approximative, a more detailed analysis of the bond topology will be made with the theoretical results.

Table 4 lists the theoretically obtained (AIM2000) bond descriptors of the $Co-C_{ax}$ and $Co-N_{eq/ax}$ bcps of the model compounds (CNCbl, MeCbl and AdoCbl) at experimental geometry. The results for the optimized geometries are similar, disregarding the already mentioned differences in the two axial Co−X bond lengths. Generally, results from the optimizations are included in the text only if they provide further information. In Table 4, the corresponding values for the covalent C−C bond in ethane and the ionic bond in sodium fluoride are also given,[45] together with the values of the Co−C bond in two cobalt carbonyl complexes, one being neutral[86] and one carrying a charge of $-1e$.[45] In the neutral complex, three chemically equivalent bonds have been averaged.

By arranging all data according to the bond types, it is interesting to note that, considering $\rho(\mathbf{r}_{bcp})$, for all axial Co-X (X = C, N) bonds, a specific order of CNCbl > MeCbl > AdoCbl appears. In contrast, all similar equatorial Co−N bonds are virtually identical, ruling out a cis electronic effect, which was suggested by the experimental results. The $\rho(\mathbf{r}_{bcp})$ value on the $Co-C_{ax}$ bond is larger than on both $Co-N_{eq}$ bonds in the case

TABLE 2: Important Bond Lengths (Å) and Angles (°) of the Cobalamin Models at Experimental and Optimized Geometries

	experimental results			optimized geometries		
	CNCbl	MeCbl	AdoCbl	CNCbl	MeCbl	AdoCbl
Co−C_{ax}	1.872(1)	1.987(1)	2.021(1)	1.855	1.987	2.020
Co−N_{ax}	2.046(1)	2.157(1)	2.236(1)	2.128	2.263	2.306
Co−N21	1.886(1)	1.879(1)	1.876(1)	1.892	1.877	1.880
Co−N22	1.919(1)	1.911(1)	1.913(1)	1.943	1.934	1.933
Co−N23	1.922(1)	1.911(1)	1.899(1)	1.947	1.936	1.928
Co−N24	1.899(1)	1.875(1)	1.882(1)	1.884	1.872	1.872
N21−Co−N22	90.2(1)	89.6(1)	90.4(1)	90.30	90.14	89.95
N21−Co−N23	173.0(1)	173.7(1)	172.9(1)	173.37	173.14	172.72
N21−Co−N24	83.3(1)	83.4(1)	83.0(1)	83.12	83.19	83.04
N22−Co−N23	96.5(1)	96.6(1)	96.3(1)	96.28	96.28	96.22
N22−Co−N24	172.2(1)	171.6(1)	172.8(1)	171.79	172.51	172.73
N23−Co−N24	90.1(1)	90.6(1)	90.5(1)	90.39	90.53	90.91
N21−Co−C_{ax}	91.3(1)	92.7(1)	92.5(1)	90.95	92.94	91.62
N22−Co−C_{ax}	88.4(1)	86.9(1)	84.5(1)	87.53	87.16	88.14
N23−Co−C_{ax}	90.7(1)	89.2(1)	90.5(1)	90.13	89.78	92.44
N24−Co−C_{ax}	87.3(1)	88.9(1)	93.1(1)	87.68	89.77	90.14
N21−Co−N_{ax}	91.0(1)	92.4(1)	91.4(1)	90.53	89.75	88.97
N22−Co−N_{ax}	89.3(1)	90.6(1)	88.4(1)	92.98	92.05	91.08
N23−Co−N_{ax}	87.3(1)	86.0(1)	86.4(1)	88.34	87.64	87.06
N24−Co−N_{ax}	95.2(1)	94.2(1)	94.4(1)	91.99	91.33	90.70
fold angle[a]	43.6(1)	43.6(1)	40.4(1)	40.10	39.00	38.87
N_{ax}−Co−C_{ax}	176.8(1)	174.3(1)	171.9(1)	178.44	177.20	179.03
Co−C_{ax}−Y[b]	178.6(1)	109.5(1)	121.9(1)	179.19	109.49	120.03

[a] N21−C1−C19−N24. [b] Y ≡ N_{cyano} (CNCbl), H (MeCbl, largest angle), C_{ribose} (AdoCbl).

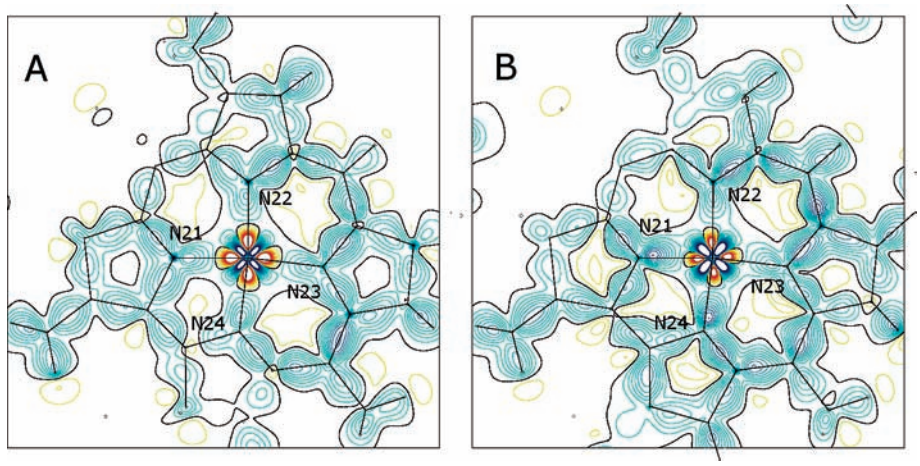

Figure 4. Experimental static deformation density maps for CNCbl (A) and AdoCbl (B) in the plane N21−Co−N22 of the corrin macrocycle (contour lines at 0.1 eÅ^{-3}).

TABLE 3: Experimentally Obtained Topological Bond Descriptors of the Co−C_{ax} and Co−$N_{eq/ax}$ Bonds (N_{eq} = N21, N22) of the Compounds CNCbl and AdoCbl

bond	$\rho(\mathbf{r}_{bcp})$, (eÅ^{-3})	$\nabla^2\rho(\mathbf{r}_{bcp})$, (eÅ^{-5})	d (Å)	d_1 (Å)	$H/\rho(\mathbf{r}_{bcp})$, (h e^{-1})	$G/\rho(\mathbf{r}_{bcp})$, (h e^{-1})
CNCbl, Co−C_{ax}	1.13(1)	5.3(1)	1.872(1)	0.921	−0.76	1.09
AdoCbl, Co−C_{ax}	0.83(2)	2.9(1)	2.021(1)	0.980	−0.62	0.87
CNCbl, Co−N21	0.83(1)	11.8(1)	1.886(1)	0.904	−0.38	1.37
AdoCbl, Co−N21	0.95(1)	11.9(1)	1.876(1)	0.913	−0.49	1.36
CNCbl, Co−N22	0.76(1)	10.6(1)	1.920(1)	0.921	−0.34	1.32
AdoCbl, Co−N22	0.83(1)	9.8(1)	1.913(1)	0.936	−0.43	1.26
CNCbl, Co−N_{ax}	0.57(1)	8.7(1)	2.048(1)	0.987	−0.20	1.26
AdoCbl, Co−N_{ax}	0.40(1)	4.6(1)	2.236(1)	1.078	−0.17	0.98

For all Co−X bonds (X = C, N) $\rho(\mathbf{r}_{bcp})$ is the electron density at the bcp; $\nabla^2\rho(\mathbf{r}_{bcp})$ is the corresponding Laplacian; d and d_1 are the bond lengths and the distances between the Co-atom and the bcp, respectively; and $H/\rho(\mathbf{r}_{bcp})$ and $G/\rho(\mathbf{r}_{bcp})$ are the total and kinetic energy densities at the bcp as derived by Abramov's relation divided by the corresponding electron density.

of CNCbl and smaller in the case of AdoCbl, as was found for the experimental results. The $\rho(\mathbf{r}_{bcp})$ value for the Co−C_{ax} bond in MeCbl lies in between the two different Co−N_{eq} bonds. The ED at the bcps of the Co−C bonds in cobalt carbonyls is generally larger than in cyano or alkyl complexes, which is supported by the increasing bond length in the order Co−CO < Co−CN < Co−C_{alkyl}.

The Laplacian of the ED at the bcp is clearly negative for the C−C bond in ethane, as expected for a shared interaction, and positive for the ionic Na−F bond. But for transition metal

TABLE 4: Topological Bond Descriptors of the Co−C_{ax} and Co−N_{ax} Bonds in the Three Model Compounds at Experimental Geometries (AIM2000) Compared to Values for Other Bond Types

bond	$\rho(\mathbf{r}_{bcp})$ (eÅ^{-3})	$\nabla^2\rho(\mathbf{r}_{bcp})$ (eÅ^{-5})	d (Å)	d_1 (Å)	H/$\rho(\mathbf{r}_{bcp})$ (h e^{-1})	G/$\rho(\mathbf{r}_{bcp})$ (h e^{-1})	δ(A, B)	$\oint_{A\cap B}$ (eÅ^{-1})
H_3C-CH_3[a]	1.62	−13.6	1.532	0.766	−0.84	0.26	1.01	2.16
$[Co-(CO)_4]^-$[a]	1.01	13.9	1.774	0.915	−0.39	1.35	1.23	2.14
$\langle Co-(CO)_3\rangle$[b]	0.98(3)	13.4(5)	1.79(1)	0.917(1)	−0.38(1)	1.33(2)		
CNCbl, Co−C_{ax}	0.88	6.4	1.867	0.927	−0.44	0.95	0.84	2.15
MeCbl, Co−C_{ax}	0.75	1.8	1.987	0.979	−0.42	0.59	0.86	2.10
AdoCbl, Co−C_{ax}	0.70	2.1	2.021	1.016	−0.38	0.59	0.83	
CNCbl, Co−N21	0.79	11.8	1.881	0.907	−0.28	1.37	0.69	1.71
MeCbl, Co−N21	0.78	12.6	1.878	0.904	−0.27	1.40	0.69	1.68
AdoCbl, Co−N21	0.79	12.5	1.876	0.904	−0.28	1.37	0.70	1.71
CNCbl, Co−N22	0.72	10.7	1.919	0.922	−0.27	1.31	0.66	1.67
MeCbl, Co−N22	0.72	11.5	1.910	0.917	−0.26	1.37	0.65	1.68
AdoCbl, Co−N22	0.71	11.3	1.916	0.919	−0.20	1.42	0.68	1.74
CNCbl, Co−N_{ax}	0.53	8.0	2.039	0.970	−0.22	1.29	0.46	1.54
MeCbl, Co−N_{ax}	0.41	5.9	2.157	1.027	−0.19	1.20	0.35	1.24
AdoCbl, Co−N_{ax}	0.34	4.7	2.234	1.058	−0.14	1.13	0.31	1.08
Na−F[a]	0.29	8.6	1.986	0.923	0.29	1.79	0.46	0.46

[a] Results taken from ref 45. [b] Results taken from ref 86. [c] δ(A, B) is the delocalization index; $\oint_{A\cap B}$ is the integrated amount of electrons within the zero flux surface. For all other quantities, see Table 3.

complexes (TM complexes), this relation does not hold anymore because the bcp is always in a region of charge depletion, so positive values do not clearly indicate an ionic bond.[45] Therefore, further descriptors which provide deeper insight into the strength and character of the Co−C_{ax} and Co−$N_{eq/ax}$ bonds of the Cbl's were established in ED studies.

The Laplacian $\nabla^2\rho(\mathbf{r})$ is linked to the kinetic energy density $G(\mathbf{r})$ (everywhere positive) and to the potential energy density $V(\mathbf{r})$ (everywhere negative) at each point $\mathbf{r}$ by a local virial theorem.[46] Both properties show different behavior in different bond types[87,45] and are therefore used in topological analyses of TM complexes. $V(\mathbf{r})$ dominates in covalent and dative bonds so that the total energy density ($H(\mathbf{r}) = G(\mathbf{r}) + V(\mathbf{r})$) becomes negative at the bcp. All Co−C_{ax} and Co−$N_{eq/ax}$ bcp's have negative values (see Table 4) but lie clearly above the $H(\mathbf{r})$ value obtained for the C−C bond in ethane, thus revealing their character as dative bonds. According to Espinosa et al., these bonds are in the *transit* region between covalent and ionic, which means they are closed shell interactions.[87] Since $G(\mathbf{r})$ is related to the Pauli repulsion, the $G(\mathbf{r})/\rho(\mathbf{r})$ ratio increases in cases of more polar bonds where the interatomic surface of zero flux (ZFS) is shifted to a significant degree toward the electropositive atom and penetrates into its atomic core region. This is reflected in the d_1 values. Regarding all Co−X bonds given in Table 4, the following order considering the $G(\mathbf{r})/\rho(\mathbf{r}_{bcp})$ values is found: Co−(CO) ≈ Co−N > Co−(CN) > Co−C_{alkyl}. The $G(\mathbf{r})/\rho(\mathbf{r}_{bcp})$ values of the Co−N bonds are larger than for Co−(CN) and Co−C_{alkyl}, although they are longer, because the N atoms are more electronegative than carbon. The most sensitive descriptor is $H(\mathbf{r})/\rho(\mathbf{r})$, which divides the data into three classes: the smallest values for the Co−C_{ax} bond, the intermediate values for the Co−N_{eq} bonds, and the largest values for the Co−N_{ax} bonds. The smaller values for $H(\mathbf{r})/\rho(\mathbf{r})$ in the carbonyl complexes compared to the cobalamines are related to their larger $G(\mathbf{r})$ values.

Both the delocalization index δ(Co, C) and the integrated number of electrons within the ZFS ($\oint_{Co\cap C}$) support covalent contributions for all given Co−C bonds, since all values are close to the values of the C−C bond. Moreover, both parameters classify the bond types in the same order that was found for $H(\mathbf{r})/\rho(\mathbf{r})$.

The number of electron pairs shared between the metal atom and the oxygen atom in carbonyl clusters as given by δ(Co, O_{CO}) is discussed in the literature as an indication of π-backbonding.[45] Those values vary from 0.09 to 0.22 in the given examples. For the cyano ligand, the corresponding value is $\delta(Co,N_{CN}) = 0.15$, revealing also significant π-backdonation from Co to CN. This is supported by the results of the ELI, which will be disussed below, and earlier findings that revealed a Mulliken Co−C bond order of 0.25 for CNCbl, in contrast to 0.13 and 0.15 for MeCbl and AdoCbl, respectively.[36] Comparison of the bond length of the CN bond in the free cyano ligand (CN^-) and CNCbl, both obtained by geometry optimization at the same level of theory, reveals a shortening of about 0.01 Å in CNCbl (1.174 Å compared to 1.186 Å in CN^-) which is contradictory to the π-backdonation. Furthermore, the CN-stretch frequency νCN of vitamin B_{12} is found to be slightly shifted to higher energies as compared to the free cyanid anion (2137 cm^{-1} in CNCbl compared to 2080 cm^{-1} in KCN).[89] However, in a NMR study of cobaloximes, evidence for cobalt-to-cyanide π-bonding was made,[90] so we believe that the value of the νCN frequency is not a sufficient criterion for the exclusion/confirmation of π-backdonation from the metal to the cyano ligand. The reason is that the orbital energies of the C atom shift to lower values in the process of building the Co−C bond, coming closer to the values of the N atom. This leads to a higher degree of covalency in the CN bond and, thus, to a shortening of the bond length. This may overrule the effect of the π-backbonding.

The distortions of the VSCCs due to bond formation provide a qualitative indication of the bond type. Figure 5A displays the Laplacian for CNCbl of the model at experimental geometry in a plane perpendicular to the corrin macrocycle, including the Co atom and parts of both axial ligands. The corresponding static deformation map shows the related features (see Figure 5B).

Covalent bonds have two (3, −3) critical points in $\nabla^2\rho(\mathbf{r})$ between the bonded atoms, whereas donor−acceptor interactions generally show the already mentioned "key-lock" arrangement, with a pronounced charge depletion at the metal site.[75] This is also found here. The topology in $\nabla^2\rho(\mathbf{r})$ around the Co atom almost matches an [8, 12, 6] cuboidal shape, which is common for TM complexes[45] (see Figure 5B). Eight (3, −3) charge concentrations are located at the corners of the distorted cube, 12 (3, −1) saddle points are at the midpoints of the edges, and 6 charge depletions face the ligands (which means they are in

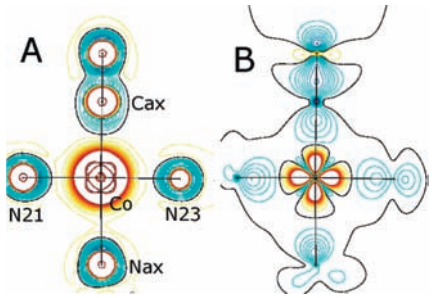

Figure 5. Results of the multipole refinement of the theoretically obtained structure factors for CNCbl; model at experimental geometry. (A) Representation of the Laplacian of the electron density perpendicular to the corrin plane, including the axial Co−C and Co−N bonds (contour lines at 5 eÅ^{-5}; blue, negative values; red, positive values). (B) Corresponding static deformation density map (contour lines at 0.1 eÅ^{-3}; blue, positive values; red, negative values).

the center of the cube faces). The cubic shape of the Co atoms is also represented in the monosynaptic valence basins of the Co atom within the ELI-D partitioning scheme (see Figures 7), which will be discussed below. Since the Co atom is centered in a distorted octahedran ligand sphere, the $\rho(\mathbf{r}_{bcp})$ and $\nabla^2\rho(\mathbf{r})$ values are not equal at all critical points, but similar. The averaged $\rho(\mathbf{r}_{bcp})$ values at the (3, −3) cps in $\nabla^2\rho(\mathbf{r})$ of the ligand C atoms of the Co−C bond show small differences between the cyano derivative and the alkyl forms, being 1.90, 1.64, and 1.65 (eÅ^{-3}) for CNCbl, MeCbl, and AdoCbl, respectively. This is also reflected in the VSCCs of the Co atom (31.15, 30.89, and 30.88 eÅ^{-3} for CNCbl, MeCbl, and AdoCbl).

The overall differences between AdoCbl and MeCbl are very small, indicating a similar bonding situation in both compounds, whereas the bond to the more electronegative cyano ligand is stronger and more polar.

d-Orbital Occupancies. For transition metal atoms, the d-orbital occupancies can be derived from multipole population parameters[88] under the assumption that they can be represented by single Slater-type orbitals and that the overlap between metal and ligand atoms is small, which is less satisfied for strong σ-donors, such as CN and alkyl ligands. Nevertheless, this approach was widely used in TM studies.[91] The d-orbital analysis generally shows nonzero populations for these orbitals, which are destabilized in terms of ligand field effects (z^2 and $x^2 - y^2$ in the case of an octahedral ligand field). This is an indication of significant covalent contributions (σ-donation) in the M−L interactions. Thus, populations of the destabilized orbitals do not contradict the fact that all three molecules are low-spin and diamagnetic. Another important aspect for these complex systems is the mixing of excited configurations, which has been analyzed for cobalt porphyrine[48] and phtalocyanine[55] complexes and was also found in a spectroscopic and computational study on Co^{3+} corrinoids.[9] This mixing leads to noninteger populations in the metal d-orbitals.

The relative occupancies of the d-orbitals are much less sensitive to the choice of the radial functions. However, since it is common practice to present also the absolute values, both absolute and relative numbers for the three models are given in Table 5. Furthermore, the experimentally obtained results and the values for octahedral Co(III) and Fe(II) complexes from the literature (see Table 5) are included. The numbers in parentheses give the percentage populations. The population errors for the experimental cases are not given; they were estimated to be around 0.1*e* (see, for example, ref 49). Furthermore, the expected values for the free ions ($Co^{3+} \equiv Fe^{2+}$) are included.

Regarding the theoretical results of the Cbl's, one finds that the total d-orbital populations slightly increase in the direction CNCbl < AdoCbl ≈ MeCbl and that the same trend is found in the z^2-orbital, which is directed toward the β-ligand. This may be related to the π back-donation of the cyano ligand, which weakens the effect of the σ donation. The fact that MeCbl overrules AdoCbl slightly may be attributed to the sterical hindrance of the adenosyl fragment, which prevents maximum overlap of the C(sp^3) and Co(d^2) orbitals.

Comparison with experimental results of other nearly octahedral formal $3d^6$ complexes reveals remarkable overall agreement with the percentage distributions in $Co(CN)_6^{3-}$,[44] $Co(NH_3)_6^{3+}$ [44] and Iron(II) *meso*-tetraphenylporphyrin bis(pyridine) [Fe(II)TPP(Pyr)$_2$].[54] The observed trend considering the z^2-orbital occupation is as follows: alkyl (strong σ-donor), cyano (strong σ-donor and weak π-acceptor), NX_n (weak σ-donor). All mentioned complexes are low-spin. In contrast, the iron(II) tetraphenylporphyrin bis(tetrahydrofuran) [Fe(II)TPP(THF)$_2$][52] has a high-spin configuration, which results in a significantly lower total population and increased e_g-orbital occupancy.

The metal atom of iron(II) tetraphenylporphyrin [Fe(II)TPP][51] is embedded in a square-planar ligand field due to the absence of axial ligands. The low-lying z^2-orbital is therefore populated with nearly two electrons. The differences between the octahedral cases and the square-planar case, as well as the differences between low-spin and high-spin states, give an impression of how the theoretical XD refinements fit into accepted concepts. This comparison reveals that small changes, such as interchange of an axial ligand, generate only the smallest changes in the d-orbital populations, differences which could hardly be seen in the experiment. However, although the absolute numbers are systematically larger in the experimental cases, the percentage values are quite similar to the theoretical results.

Atomic Properties. It turned out that although the bond topological properties are quite insensitive to the quality of the experimental data, the integrated atomic properties are not. Especially, the charges of the Co atom are in the region of +0.80 e for AdoCbl and +0.05 e for CNCbl, slightly dependent on the inclusion of theoretical expansion/contraction parameters. To examine whether these effects are just a matter of numerical accuracy, the Co atoms were reintegrated with a much smaller stepsize, which did not change the results significantly. Additional procedures, such as introduction of anisotropic thermal parameters for the H atoms[92] and exclusion of such low-order reflections that differ more than an arbitrarily chosen value from the F_{calc} (see, for example, ref 93), did not lead to reliable atomic properties. Problems with experimentally obtained atomic properties of transition metals are known.[93] Because of these large uncertainties, only theoretical results are discussed.

Table 6 shows the theoretically obtained atomic charges of the models at experimental geometry. The AIM charges of the Co atoms were obtained by the program AIM2000; all other atoms were integrated with Basin4.3. Due to the fact that the axial Co−C and Co−N bonds are the major scope of this study and that various approaches to obtain atomic charges are discussed in the literature,[94,95] only summed-up values for the functional groups within the models are given. It has been stated that "the charges of appropriate groups of atoms are conserved more consistently than are those of the individual atoms".[96] The same is found here for different theoretical approaches. The most common approaches, AIM and natural population analysis (NPA), are compared. The axial ligands as well as the Co atom and corrin ring are suggested to be functional groups in the

TABLE 5: d-Orbital Populations of the Co Atoms for the Three Cobalamines (Calculations at Experimental Geometries and Experimental Results) and Complexes of Co^{3+} and Fe^{2+} [a]

	theory at experimental geometries			experimental results		
	CNCbl	MeCbl	AdoCbl	CNCbl	MeCbl	AdoCbl
z^2	0.97 (14)	1.04 (15)	1.02 (15)	1.21 (16)		1.21 (16)
$x^2 - y^2$	0.90 (13)	0.89 (13)	0.83 (12)	0.88 (12)		1.11 (14)
sum 1[b]	1.87 (27)	1.93 (28)	1.85 (27)	2.09 (28)		2.32 (30)
xy	1.69 (25)	1.75 (25)	1.75 (25)	1.84 (24)		1.96 (26)
xz	1.63 (24)	1.60 (23)	1.64 (24)	1.87 (24)		1.75 (22)
yz	1.63 (24)	1.60 (23)	1.64 (24)	1.87 (24)		1.75 (22)
sum 2[c]	4.95 (73)	4.95 (72)	5.03 (73)	5.60 (72)		5.48 (70)
total	6.82	6.89	6.88	7.67		7.78
	$Co(CN)_6^{3-}$ [44]	$Co(NH_3)_6^{3+}$ [44]	Fe(II)TPP$(Pyr)_2$[54]	Fe(II)TPP$(THF)_2$[52]	Co^{3+}, Fe^{2+} spherical	Fe(II)TPP[51]
z^2	0.94 (13)	0.87 (12)	0.72 (10)	1.04 (18)	1.2 (20)	1.70 (24)
$x^2 - y^2$	0.94 (13)	0.87 (12)	0.81 (11)	1.42 (24)	1.2 (20)	0.43 (6)
sum 1[b]	1.88 (26)	1.74 (24)	1.53 (21)	2.46 (42)		
xy	1.82 (25)	1.81 (24)	1.99 (27)	0.93 (16)	1.2 (20)	1.50 (21)
xz	1.79 (25)	1.94 (26)	1.93 (26)	1.26 (21)	1.2 (20)	1.77 (25)
yz	1.79 (25)	1.94 (26)	1.93 (26)	1.26 (21)	1.2 (20)	1.77 (25)
sum 2[c]	5.40 (75)	5.69 (77)	5.85 (79)	3.45 (58)		
total	7.26	7.44	7.40	5.92	6.0	7.17

[a] Numbers in parentheses give the percentage values. [b] $z^2 + (x^2 - y^2)$. [c] $xy + xz + yz$.

TABLE 6: AIM and NPA Charges (in *e*) of the Functional Groups (α-Ligand, Co Atom, Corrin Ring, *β*-Ligand) of the Three Model Compounds at Experimental Geometries[a]

	CNCbl		MeCbl		AdoCbl	
	AIM	NPA	AIM	NPA	AIM	NPA
β [C_{ax}]	−0.48 [0.74]	−0.35 [0.09]	−0.13 [−0.10]	−0.10 [−0.67]	−0.15 [−0.11]	−0.11 [−0.46]
Co	1.12	0.68	1.07	0.73	1.07	0.75
corrin	0.22	0.47	−0.13	0.22	−0.04	0.23
α [N_{ax}]	0.18 [−1.04]	0.21 [−0.44]	0.09 [−1.03]	0.14 [−0.45]	0.11 [−1.03]	0.14 [−0.45]
total	1.04	1.00	0.90	1.00	0.99	1.00

[a] Charges of the (Co−)C_{ax} and the (Co−)N_{ax} atoms in square brackets.

B12 cofactors. Additionally, the values for the (Co−)C_{ax} and (Co−)N_{ax} atoms of the three models are listed. They are given in square brackets, because they do not contribute separately to the total charge given in the last line of Table 6 because they belong to the β and α ligands.

As expected, the general trends are comparable between both approaches in terms of functional groups. The charge difference between AIM and NPA never exceeds 0.35 e for the corrin ring and the axial ligands. Considering single atoms, the situation is quite inconsistent. It is known for early main group elements[68] that AIM charges are generally larger than NPA charges. This is also found for the Co atom, but interestingly, not for the (Co−)C_{ax} atoms in MeCbl and AdoCbl, where AIM predicts less negative charges than NPA. The fact that the nature of the β-ligand does not affect the net charge of the Co atom and the other five N donors (not shown) agrees with earlier findings.[36] The Mulliken charges presented there are very similar to the NPA charges presented in this study.

The results for MeCbl and AdoCbl are practically indistinguishable in terms of AIM and, considering functional groups, also in terms of NPA. Only the (Co−)C_{ax} shows a decrease from −0.67 to −0.46*e* for the NPA charges. The charges of CNCbl show small differences from the alkylderivatives: Because the cyano ligand is σ donor and π acceptor, it is approximately 0.25−0.35*e* more negative than methyl and adenosyl. This results in slight depletions of charge at the Co atom (approximately 0.05*e*), α ligand (approximately 0.07*e*) and corrin (∼0.25*e*), respectively. Although the effects are quite small, the fact that the corrin ring mainly balances the charge demands of the β-ligand points toward intense electronic comunication between the macrocycle and the axial ligands, as found earlier (see ref 9 and references therein).

Source Function. A recently developed tool to investigate ED-derived properties of chemical bonds is the source function. In covalent bonds, the two direct bond partners generally contribute over 80% to the ED at the bcp.[97] In TM complexes, the situation is different.[76] As for the atomic charges, only summed-up values are given for the functional groups in Table 7, which includes both the results of the models at experimentally derived geometries and those from geometry optimizations. Reference points are the Co−C_{ax} and Co−N_{ax} bcp's. All numbers are given as percentage contributions. The contributions from the Co atom and the direct bond partner (C and N, respectively) are positive and in the same order of magnitude for all investigated Co−C_{ax} and Co−$N_{eq/ax}$ bonds.

The calculated contributions do not sum up to 100%, but vary between 90 and 110%, so that the data were scaled to 100%. Therefore, trends can be clearly detected for the integration results of the optimized geometries (right side of Table 7), since there, the variance is significantly smaller (1−5%). The results for the models based on experimental geometries do not provide unambiguous data. However, the overall agreement among the trends is reasonable. Generally, the results may be improved in accuracy with smaller integration increments, but this is not feasible for models with at least 80 atoms. It is even less feasible for the complete structure due to the size of the molecules.

However, regarding the Co−C_{ax} bond, some interesting trends appear. The contributions from the β-ligand and the Co atom to the ED at the bcp decrease continuously from CNCbl to AdoCbl. The decrease for the (Co−)C atom is even larger (given

TABLE 7: Integrated Source Function of the Functional Groups (α-Ligand, Co Atom, Corrin Ring, *β*-Ligand) to the Co−C_{ax} and Co−N_{ax} Bond Critical Points for the Three Model Compounds at Experimental and Optimized Geometries[a]

	experimental geometries			optimized geometries		
	CNCbl	MeCbl	AdoCbl	CNCbl	MeCbl	AdoCbl
Co−C_{ax}						
β [Co − C]	46 [31]	48 [28]	44 [24]	48 [33]	46 [29]	45 [27]
Co	30	28	28	34	31	30
corrin	22	21	26	16	22	24
α	2	3	2	2	1	1
Co−N_{ax}						
β	6	6	6	6	6	5
Co	16	14	11	14	9	6
corrin	35	32	41	26	41	40
α [Co − N]	43 [21]	48 [20]	42 [16]	54 [18]	44 [13]	49 [13]

[a] Contributions of the (Co-)C_{ax} and the (Co-)N_{ax} atoms in square brackets.

in brackets), so that the contributions of the direct bond partners Co and C decrease from 67% (CNCbl) to 57% (AdoCbl), accompanied by an increase in contribution from the corrin ring. The minor influence of the α-ligand does not change by exchange of the *β*-ligand, supporting earlier findings that the α-ligand has negligible electronic impact on the Co−C_{ax} bond.[9,10]

The opposite holds for the Co−N_{ax} bcp. Here, the *β*-ligand shows a larger contribution, also independent of the ligand type. This is a clear hint to the inverse trans-axial electronic effect, discussed in the literature and related to the stronger *σ*-donation of C residues as compared to N residues. The Co−N_{ax} bond is the weakest and longest Co−X bond in all three compounds. This is reflected by the SF. The direct bond partners Co and N contribute only 32% in the case of CNCbl, decreasing even further to 22 and 19% for MeCbl and AdoCbl, respectively. In contrast, the corrin contribution increases dramatically from 26 to 41/40%, which means the main part of the ED at the Co−N_{ax} bcp originates from the corrin ring and not from the Co and N atoms in the two alkylderivatives. These results reveal the complex electronic situation in this class of compounds.

For the Co−N_{eq} bonds (not shown), a contribution of approximately 5% from the *β*-ligand to the bcp is found for all six models, also independent of the ligand type, which points toward the already mentioned cis electronic effect of the *β*-ligand. In the bond topological properties, this effect was not visible.

The local source (LS) is a qualitative indication whether a given point in space (or a set of points along a line) is acting as source or sink for the ED at any chosen reference point (rp) and to what degree.[98] Mostly, a bcp is chosen as rp because it is regarded to be the less biased choice.[97] For the same reason, the bond path is chosen for the line of points for which the LS is calculated relative to the rp. Alternatively, the line connecting the two atoms is used,[93] which is easier to compute and justified in cases that both trajectories nearly fall together. The latter possibility was chosen in this study.

Covalent bonds show positive values of the LS in the region around the bcp, which means these points act as a source for the ED at the bcp. In heteropolar cases, this distribution shows asymmetry dependent on the difference of electronegativities (ΔEN) between both atoms, which is discussed as a measure of bond polarity.[98] Figure 6A and B show the distribution of $\nabla^2\rho(\mathbf{r})$ and LS along the Co−C_{ax} line for AdoCbl and CNCbl. $\nabla^2\rho(\mathbf{r})$ and LS are similar for AdoCbl and MeCbl; therefore, the latter one is not displayed. In both cases, the outer shell of the Co atom acts as a sink, whereas the outer shell of the carbon atom supplies ED to the bcp. The asymmetry is higher in the case of CNCbl, which is in line with the higher $G/\rho(\mathbf{r}_{bcp})$ value for CNCbl as compared to the alkyl derivatives. In terms of the LS, the Co−C_{ax} bond is a closed shell interaction, but since the LS is restricted to the trend of $\nabla^2\rho(\mathbf{r})$, which was found to be insufficient to describe the bond type of TM−X bonds (disappearance of the outer shell), these results have to be considered with care. The bcp lies in a region where $\nabla^2\rho(\mathbf{r})$ changes rapidly (CNCbl) and small changes in d_1 may switch the sign of $\nabla^2\rho(\mathbf{r})$ at the bcp's position. In a recent paper, this crossover from closed-shell to shared interaction was shown for second-row hydrides, H−Be to H−B, the former one being discussed as closed-shell, the latter as covalent.[98] In both cases, the point where $\nabla^2\rho(\mathbf{r})$ changes its sign lies very close to the bcp.

The situation is different for the Co−N_{ax} bonds (see Figure 6C, (AdoCbl)). The asymmetry is slightly smaller compared to the corresponding Co−C_{ax} bond (Figure 6A) because the orbital overlap is smaller in the Co−N_{ax} bond. Due to the large bond distance, the electronic situation at the bcp is dominated mainly by the Laplacian of the Co atom, which leads to a significantly longer distance between bcp and the sign-change point because $\nabla^2\rho(\mathbf{r})$ is flat in the region of the bcp. The electron pair of the nitrogen atom which forms a dative bond to the Co atom is highly localized and contributes ED to the bcp.

Electron Localizability Indicator. Following Bader, covalent, dative, and metallic bonds are subclasses of the shared interaction.[46] In such interactions, an attractor (point or ring) is found in the localization function between neighboring atoms, which is not the case for closed-shell interactions. The fact that the ELI-D-attractors of the Co−C_{ax} and Co−N_{ax} bonds lie very close to the Co−X line (<0.1 Å for all cases) reveals their dative character. Figure 7 displays an isosurface of the ELI-D (η = 2.0) of CNCbl and AdoCbl (Moliso representation).[99] The region around the Co−C_{ax} bond is highlighted by a red circle. The shape of the V_2 (Co, C_{ax}) is toroid in CNCbl. As for TM-carbonyls, this points toward *π*-backbonding contributions:[100,101] the shape of the alkyl derivatives matches that of single bonds. In AdoCbl, a distortion toward the nonbonded electron pair of the O atom in the ribose ring is found, which is highlighted by a horizontal arrow. This reflects the impact of the steric repulsion between adenosyl fragment and corrin ring (highlighted by the upright arrow) to the density overlap between the Co and the C atom. This distortion is not found in MeCbl (not shown). Interestingly, it is retained in the optimized model of AdoCbl, which lacks the sterically demanding amide side chains. The unsaturated structure of the corrin macrocycle and the DMB is reflected by the shape and volume of the disynaptic bond basins in the rings.

The outer core shell of the Co atom shows the expected splitting[102] into a set of eight basins (see Figure 7) located in the same areas as the electron accumulations in the static deformation density maps and the VSCCs around the Co atom. Within the framework of ELI-D, these accumulations can be quantified in terms of electron numbers. The outer core shell for first-row TM complexes is $n = 3$ (n = main quantum number). The population of the 4s electrons is distributed over the disynaptic valence basins connecting Co with the other atoms and is, therefore, hard to quantify. Nevertheless, the third shell may allow statements on the oxidation state of the TM in certain cases, since the number of 3d electrons can be counted. Due to

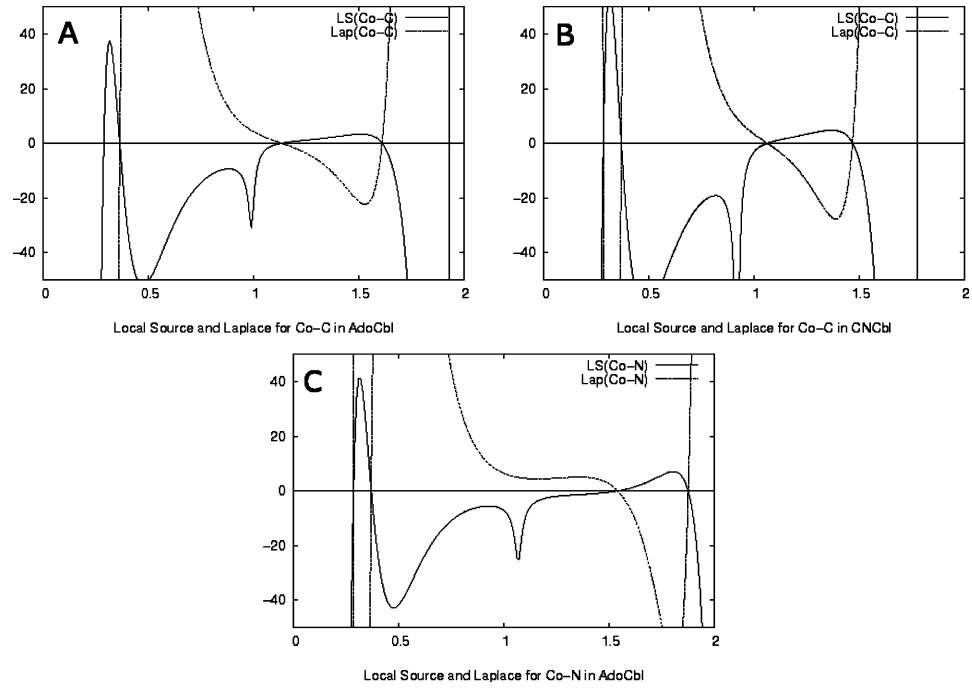

Figure 6. Laplacian (Lap) and corresponding LS distribution of the Co−C_{ax} bond in AdoCbl (A) and CNCbl (B) and of the Co−N_{ax} bond in AdoCbl (C); models at experimental geometries.

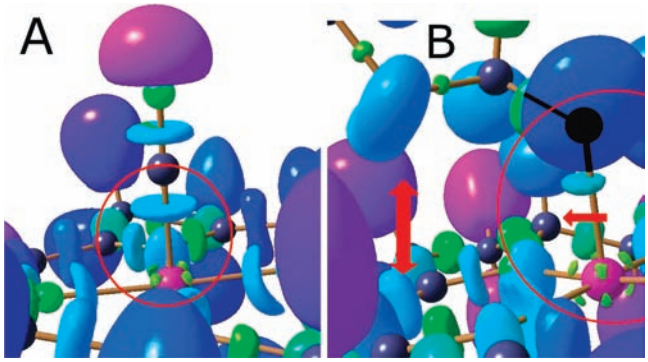

Figure 7. Moliso representations of the ELI-D in CNCbl (A) and AdoCbl (B); isocontour value of the ELI-D: $\eta = 2.0$; models at experimental geometries. The regions around the Co−C_{ax} bond are highlighted by red circles. In AdoCbl, the corresponding (Co−)C_{ax} is given as a shadow representation, because it is covered by its protonated valence basins. The two arrows in B highlight the steric repulsion between the nonbonded electron pair of the O atom in the ribose moiety and the corrin ring (upright arrow) and the corresponding distortion of the disynaptic valence basin V_2 (Co, C_{ax}) (horizontal arrow).

orbital overlap, the obtained numbers are never equal to the expected integer values following from the Aufbau principle. Fortunately, the expected values in terms of ELF (and also ELI-D, as long as electron correlation is not taken into account) have been calculated for the free atoms.[103] Table 8 lists the core shell and valence populations for the Co atoms in the three Cbl's. The comparison to the values for the free Co atom affirm the quality of the integrations. Complete lists for all basins are given in the supplement. The outer core shell shows only little differences among CNCbl, MeCbl, and AdoCbl, but the fact that CNCbl has the smallest number of electrons in the 3d shell may be related to the π-backbonding effect.

Considering V_2 (Co, C_{ax}), the basin in CNCbl contains significantly more electrons, which also reflects the π-backbonding. The alkyl derivatives show comparable populations in this bond. Both basins are highly unsaturated.[63] The percentage volume and population distribution of V_2 (Co, C_{ax}), that is,

TABLE 8: Integrated ELI-D Populations (in *e*) for the Core Shells, the Co−C_{ax}, and the Co−N_{ax} Bond Basins of the Three Model Compounds at Experimental Geometries[a]

	CNCbl	MeCbl	AdoCbl	free Co[b]
Co_{core}, $n = 1$	2.24	2.24	2.24	2.2
Co_{core}, $n = 2$	8.17	8.18	8.17	8.2
Co_{core}, $n = 3$	14.42	14.47	14.58	14.3
V_2 (Co, C_{ax})	2.20	1.24	1.33	
$\%_{Vol}$ (Co)	20	37	30	
$J_{(M-C)_{pop}}$ (%)	0.33 (15)	0.33 (27)	0.33 (25)	
V_2 (Co, N_{ax})	2.89	2.84	2.99	
$\%_{Vol}$ (Co)	8	7	5	
$J_{(M-C)_{pop}}$ (%)	0.11 (4)	0.08 (3)	0.07 (2)	

[a] V_2 (Co, C_{ax}) is the electron population of the disynaptic valence basin of the Co−C bond, $\%_{Vol}$ (Co) is the volume fraction of this basin inside the Co atomic basin, $J_{(M-C)_{pop}}$ (%) is the Jansen index, which gives the corresponding absolute [relative] electron numbers of this fraction. [b] Values taken from ref 103.

the ELI-D and AIM partitioning, are combined to provide a measure of how the bond is polarized toward one atom[104] and give further insight into the bonding situation. This is called the Jansen index $J_{(M-C)_{pop}}$ (%) and was already applied to metal−carbon (M = K−Mn) bonds in a theoretical study,[105] also including methyl-metals. In the compounds reported,[105] $J_{(M-C)_{pop}}$ (%) increases from 7.0 (K−CH_3) to 28.3 (Mn−CH_3), revealing increasing covalent contributions. MeCbl (27) and AdoCbl (25) are in line with these results. The value for CNCbl (15) is significantly smaller, indicating a more polarized bond. Due to the already mentioned steric hindrance of the adenosyl fragment, the overlap between the carbon atom and the cobalt atom is smaller in AdoCbl, which is reflected in the smaller volume fraction of V_2 (Co, C_{ax}) within the Co atom in AdoCbl as compared to MeCbl. However, this has a negligible effect on the population distribution. The absolute and relative values for the Co−N_{ax} bonds are slightly affected by the upper ligand.

Conclusion

The experimental conditions to obtain an ED-suitable data set of one of the B_{12} cofactors are restrictive due to crystal

quality and complexity/size of these systems. Due to unavoidable experimental errors and noise, experimentally derived quantitative properties of the electron density (e.g. at the bond critical point) usually show a large variance. If the electronic differences are only small, these variances might prevent the detection of trends in the data. For the experimentally derived data given in Table 3, however, there are very distinct trends, which discriminate between the bonding types and which are also reproduced by theory (see Table 4). It should be noted that the theoretically obtained data are affected by the approximative character of the density functional and the limitations of the basis set. Therefore, not the individual values but the trends should and, indeed, do agree. Nevertheless, the quantitative results of the experiments, topology, and integrated properties are significantly below the standards obtained for experimental electron densities of small molecules, so reliable information could be extracted only from the corresponding theoretical calculations. However, the demanding high-order X-ray data collections at low temperatures lead to geometries of high quality, which served as starting geometries for all calculations.

Starting with these experimentally obtained geometries, a variety of descriptors, common as well as recently introduced, have been investigated theoretically for the three Cbl's to discover the inherent electronic differences between the $Co-C_{ax}$ bonds, which are known to undergo different reaction paths in the human body. The bond topological descriptors point toward weak polar covalent $Co-C_{ax}$ and even weaker, less covalent, and more polar $Co-N_{ax}$ bonds. This is supported by the Jansen index, which is much lower for the $Co-N_{ax}$ bonds than for $Co-C_{ax}$. In contrast to that, the local source proves the $Co-C_{ax}$ bonds to be more polar. Comparison to other studies revealed that all $Co-C_{ax}$ and $Co-N_{eq/ax}$ bonds are longer and weaker than bonds between cobalt and the carbonyl ligand, which is expected and is in line with the spectrochemical series. The decrease in the delocalization index, δ (Co, C) in the order $Co-CO > Co-C_{ax} > Co-N_{eq} > Co-N_{ax}$ quantifies these results.

Examination of the d-orbital populations from the models compared to other studies of Co^{3+} and Fe^{2+} complexes showed that the population of the energetically destabilized e_g-orbitals is not based on a high-spin state but, rather, on σ donation from the ligands.

The integrated properties (atomic charges and source function) exhibit the complex electronic "communication" between the corrin ring and the axial ligands. The ELI-D revealed unsaturated $Co-C_{ax}$ bonding basins in the case of the alkyl derivatives and, in line with the other integrated properties, supports the negligible influence of the α-ligand to the $Co-C_{ax}$ bond.

The electrostatic repulsion between the adenosyl fragment and the corrin ring is retained even after geometry optimization of the model compound lacking the amide chains due to the sterical demand of the adenosyl. This leads to small electronic differences between MeCbl and AdoCbl, which basically can be observed in the source function and the electron localizability indicator. Nevertheless, these differences are too small to cause different reaction types, so destabilization of the $Co-C_{ax}$ bond in AdoCbl by the protein−substrate complex and the possibility to build an adenosyl radical can be identified as the main reasons for the biochemical differences.

Acknowledgment. We thank the Deutsche Forschungsgemeinschaft (DFG Grant Lu 222/29-2 within SPP1178) for financial support.

Supporting Information Available: CIF files for AdoCbl, MeCbl, and CNCbl (CCDC 713291−713293). Complete bond topology of both experimental multipole refinements (AdoCbl and CNCbl). Model compounds at experimental geometry: topology of all X−X bonds (X ≠ H), atomic properties and NBO-charges, populations of the ELI basins. All models (experimental and optimized): bond topology of all Co-X bonds (X = C, N); multipole parameters of the atoms Co, N(21), N(22), N_{ax}, C_{ax}, and N_{CN} for CNCbl-exp and CNCbl-opt. Integrated properties such as charges, volumes, localization index L(Co), delocalization index δ (Co, X), and integrated amount of electron density within the zero flux surface $\oint_{Co\cap X}$. Populations of the disynaptic valence basins V_2 (X, Co). Experimental procedure. This material is available free of charge via the Internet at http://pubs.acs.org.

References and Notes

(1) Lenhert, P. G.; Hodgkin, D. C. *Nature* **1961**, *9*, 937–938.
(2) Matthews, R. G. *Acc. Chem. Res.* **2001**, *34*, 681–689.
(3) Banerjee, R. *Chem. Rev.* **2003**, *103*, 2083–2094.
(4) Hill, H. A. O.; Pratt, J. M.; Williams, R. J. P. *J. Chem. Soc.* **1965**, *515*, 2859–2865.
(5) Ludwig, M. L.; Matthews, R. G. *Annu. Rev. Biochem.* **1997**, *66*, 269–313.
(6) Halpern, J. *Science* **1985**, *227*, 869–875.
(7) Jensen, K. P.; Ryde, U. *J. Mol. Str. (Theochem)* **2002**, *585*, 239–255.
(8) Dölker, N.; Maseras, F.; Lledós, A. *J. Phys. Chem.* **2003**, *B107*, 306–315.
(9) Stich, T. A.; Brooks, A. J.; Buan, N. R.; Brunold, T. C. *J. Am. Chem. Soc.* **2003**, *125*, 5897–5914.
(10) Jensen, K. P.; Ryde, U. *J. Am. Chem. Soc.* **2005**, *127*, 9117–9128.
(11) Medek, A.; Frydman, V.; Frydman, L. *Proc. Natl. Acad. Sci. U.S.A.* **1997**, *94*, 14237–14242.
(12) Medek, A.; Frydman, L. *J. Am. Chem. Soc.* **2000**, *122*, 684–691.
(13) Ke, S.-C.; Torrent, M.; Museav, D. G.; Morokuma, K.; Warncke, K. *Biochemistry* **1999**, *38*, 12681–12689.
(14) Torrent, M.; Museav, D. G.; Morokuma, K.; Ke, S.-C.; Warncke, K. *J. Phys. Chem.* **1999**, *103*, 8618–8627.
(15) Warncke, K.; Utade, A. S. *J. Am. Chem. Soc.* **2001**, *123*, 8564–8572.
(16) Andruniow, T.; Zgierski, M., Z.; Kozlowski, P. M. *J. Phys. Chem.* **2002**, *A106*, 1365–1373.
(17) Nie, S.; Marzilli, P. A.; Marzilli, L. G.; Yu, N.-T. *J. Chem. Soc., Chem. Commun.* **1990**, 770–771.
(18) Dong, S.; Padmakumar, R.; Banerjee, R.; Spiro, T. G. *J. Am. Chem. Soc.* **1996**, *118*, 9182–9183.
(19) Birke, R. L.; Huang, Q.; Spataru, T.; Gosser, D. K., Jr. *J. Am. Chem. Soc.* **2006**, *128*, 1922–1936.
(20) Hung, R. R.; Grabowski, J. J. *J. Am. Chem. Soc.* **1999**, *121*, 1359–1364.
(21) Ouyang, L.; Randaccio, L.; Rulis, P.; Kurmaev, E. Z.; Moewes, A.; Ching, W. Y. *J. Mol. Struc. (Theochem)* **2003**, *622*, 221–227.
(22) Bouqiere, J. P.; Finney, J. L.; Lehmann, M. S.; Lindley, P. F.; Savage, H. F. J. *Acta Crystallogr.* **1993**, *B49*, 79–89.
(23) Kratky, C.; Farber, G.; Gruber, K.; Wilson, K.; Dauter, Z.; Nolting, H. F.; Konrat, R.; Kräutler, B. *J. Am. Chem. Soc.* **1995**, *117*, 4654–4670.
(24) Randaccio, L.; Furlan, M.; Geremia, S.; Slouf, M.; Srnova, I.; Toffoli, D. *Inorg. Chem.* **2000**, *39*, 3403–3413.
(25) Gruber, K.; Reitzer, R.; Kratky, C. *Angew. Chem., Int. Ed.* **2001**, *40*, 3377–3380.
(26) Mathews, F. S.; Gordon, M. M.; Chen, Z.; Rajashankar, K. R.; Ealick, S. E.; Alpers, D. H.; Sukumar, N. *Proc. Natl. Acad. Sci. U.S.A.* **2007**, *104* (44), 17311–17316.
(27) Jensen, K. P.; Mikkelsen, K. V. *Inorg. Chim. Acta* **2001**, *323*, 5–15.
(28) Jensen, K. P.; Sauer, S. P. A.; Liljefors, T.; Norrby, P. *Organometallics* **2001**, *20*, 550–556.
(29) Jensen, K. P.; Ryde, U. *ChemBioChem* **2003**, *4*, 413–424.
(30) Jensen, K. P.; Ryde, U. *J. Phys. Chem.* **2003**, *A107*, 7539–7545.
(31) Jensen, K. P.; Roos, B. O.; Ryde, U. *J. Chem. Phys.* **2007**, *126*, 014103.
(32) Dölker, N.; Maseras, F.; Lledós, A. *J. Phys. Chem.* **2001**, *105*, 7564–7571.
(33) Dölker, N.; Maseras, F.; Siegbahn, P. E. M. *Chem. Phys. Lett.* **2004**, *386*, 174–178.
(34) Dölker, N.; Morreale, A.; Maseras, F. *J. Biol. Inorg. Chem.* **2005**, *10*, 509–517.

(35) Kurmaev, E. Z.; Moewes, A.; Ouyang, L.; Randaccio, L.; Rulis, P.; Ching, W. Y.; Bach, M.; Neumann, M. *Europhys. Lett.* **2003**, *62* (4), 582–587.

(36) Ouyang, L.; Rulis, P.; Ching, W. Y. *Inorg. Chem.* **2004**, *43*, 1235–1241.

(37) Andruniow, T.; Zgierski, M. Z.; Kozlowski, P. M. *J. Phys. Chem.* **2000**, *B104*, 10921–10927.

(38) Andruniow, T.; Zgierski, M. Z.; Kozlowski, P. M. *Chem. Phys. Lett.* **2000**, *331*, 509–512.

(39) Andruniow, T.; Zgierski, M. Z.; Kozlowski, P. M. *J. Am. Chem. Soc.* **2001**, *123*, 2679–2680.

(40) Kozlowski, P. M. *Curr. Opin. Chem. Biol.* **2001**, *5*, 736–743.

(41) Freindorf, M.; Kozlowski, P. M. *J. Am. Chem. Soc.* **2004**, *126*, 1928–1929.

(42) Kozlowski, P. M.; Andruniow, T.; Jarzecki, A. A.; Zgierski, M. Z.; Spiro, T. G. *Inorg. Chem.* **2006**, *45*, 5585–5590.

(43) Hay, B. P.; Finke, R. G. *J. Am. Chem. Soc.* **1987**, *109*, 8012–8018.

(44) Iwata, M.; Saito, Y. *Acta Crystallogr.* **1973**, *B33*, 59–69.

(45) Macci, P.; Sironi, A. *Coord. Chem. Rev.* **2003**, *238*−*239*, 383–412.

(46) Bader, R. F. W. *Atoms in Molecules. A Quantum Theory*; Cambridge University Press: Oxford, U.K., 1991.

(47) Foster, J. P.; Weinhold, F. *J. Am. Chem. Soc.* **1980**, *102*, 7211–7218.

(48) Stevens, E. D. *J. Am. Chem. Soc.* **1981**, *103*, 5087.

(49) Lecomte, C.; Chadwick, D. L.; Coppens, P.; Stevens, E. D. *Inorg. Chem.* **1983**, *22*, 2982–2992.

(50) Coppens, P.; Li, L. *J. Chem. Phys.* **1984**, *81* (4), 1983–1993.

(51) Tanaka, K.; Elkaim, E.; Li, L.; Jue, Z. N.; Coppens, P. *J. Chem. Phys.* **1986**, *84* (12), 6969–6978.

(52) Lecomte, C.; Blessing, R. H.; Coppens, P.; Tabard, A. *J. Am. Chem. Soc.* **1986**, *108*, 6942–6950.

(53) Elkaim, E.; Tanaka, K.; Coppens, P. *Acta Crystallogr.* **1987**, *B43*, 457–461.

(54) Li, N.; Coppens, P.; Landrum, J. *Inorg. Chem.* **1988**, *27*, 482–488.

(55) Figgis, B. N.; Kucharski, E. S.; Reynolds, P. A. *J. Am. Chem. Soc.* **1989**, *111*, 1683–1692.

(56) Dittrich, B.; Koritsanzky, T.; Volkov, A.; Mebs, S.; Luger, P. *Angew. Chem., Int. Ed.* **2007**, *46*, 2935–2938.

(57) Bader, R. F. W.; Gatti, C. *Chem. Phys. Lett.* **1998**, *287*, 233–238.

(58) Gatti, C.; Cargnoni, F.; Bertini, L. *J. Comput. Chem.* **2002**, *24* (4), 422–436.

(59) Kohout, M. *Int. J. Quantum Chem.* **2004**, *97*, 651–658.

(60) Bader, R. F. W.; Stephens, M. E. *J. Am. Chem. Soc.* **1975**, *97*, 7391–7399.

(61) Fradera, X.; Austen, M. A.; Bader, R. F. W. *J. Phys. Chem.* **1999**, *A103*, 304–314.

(62) Becke, A. D.; Edgecombe, K. E. *J. Chem. Phys.* **1990**, *92* (9), 5397–5403.

(63) Silvi, B.; Savin, A. *Nature* **1994**, *371*, 683–686.

(64) Bentley, J. J.; Stewart, R. F. *Acta Crystallogr.* **1976**, *A32*, 910–914.

(65) Volkov, A.; Abramov, Y.; Coppens, P.; Gatti, C. *Acta Crystallogr.* **2000**, *A56*, 332–339.

(66) Volkov, A.; Coppens, P. *Acta Crystallogr.* **2001**, *A57*, 395–405.

(67) Coppens, P.; Volkov, A. *Acta Crystallogr.* **2004**, *A60*, 357–364.

(68) Henn, J.; Ilge, D.; Leusser, D.; Stalke, D.; Engels, B. *J. Phys. Chem.* **2004**, *A108*, 9442–9452.

(69) Koritsánszky, T.; Volkov, A. *Chem. Phys. Lett.* **2004**, *385*, 431–434.

(70) Volkov, A.; Macci, P.; Farrugia, L. J.; Gatti, C.; Mallinson, P.; Richter, T.; Koritsanszky, T. XD2006 a computer program for multipole refinement, topological analysis of charge densities and evaluation of intermolecular energies from experimental or theoretical structure factors; User Manual, 2006, State University of New York at Buffalo: Buffalo, NY.

(71) Hansen, N. K.; Coppens, P. *Acta Crystallogr.* **1978**, *A34*, 909–921.

(72) Wilson, A. J. C. *International Tables of Crystallography*; Kluver Academic Publishers, 1992, Vol. C.

(73) Coppens, P. *Coord. Chem. Rev.* **1985**, *65*, 285–307.

(74) Spackman, M. A.; Byrom, P. G. *Acta Crystallogr.* **1997**, *B53*, 553–564.

(75) Farrugia, L. J.; Frampton, C. S.; Howard, J. A. K.; Mallinson, P. R.; Peacock, R. D.; Smith, G. T.; Steward, B. *Acta Crystallogr.* **2006**, *62*, 236–244.

(76) Farrugia, L. J.; Evans, C.; Tegel, M. *J. Phys. Chem.* **2006**, *110*, 7952–7961.

(77) Ziegler, T. *Chem. Rev.* **1991**, *91*, 651–667.

(78) Schäfer, A.; Horn, H.; Ahlrichs, R. *J. Chem. Phys.* **1994**, *100*, 5829–5835.

(79) Frisch, M. J., et al. *Gaussian03, Rev. D.01*, Gaussian Inc.: Pittsburgh PA, 1998.

(80) Biegler-König, F.; Schönbohm, J.; Bayles, D. AIM2000 - A Program to Analyse and Visualize Atoms in Molecules. *J. Comp. Chem.* **2001**, *22*, 549–559.

(81) Jayatilaka, D.; Grimwood, D. J. *TONTO: A Fortran Based Object-Oriented System for Quantum Chemistry and Crystallography*, User Manual, 2003, University of Western Australia: Perth, Australia.

(82) Kohout, M. *DGrid and Basin*, version 4.3, Max-Planck-Institut für Chemische Physik fester Stoffe: Dresden, Germany, 2007.

(83) Burnett, M. N.; Johnson, C. K. *ORTEP-III, Oak Ridge Thermal Ellipsoid Plotting Program for Crystal Structure Illustrations*, Report ORNL-6895; Oak Ridge National Laboratory: Oak Ridge, TN, 1996.

(84) Keller, E. *SCHAKAL. A Fortran Program for the Graphical Representation of Molecular and Solid-State Structure Models*, Albert Ludwigs Universität Freiburg; Germany, 1999.

(85) Abramov, Y. A. *Acta Crystallogr.* **1997**, *A53*, 264–272.

(86) Macchi, P.; Garlaschelli, L.; Sironi, A. *J. Am. Chem. Soc.* **2002**, *124*, 14173–14184.

(87) Espinosa, E.; Alkorta, I.; Elguero, J.; Molins, E. *J. Chem. Phys.* **2002**, *117*, 5529.

(88) Holladay, A.; Leung, P.; Coppens, P. *Acta Crystallogr.* **1983**, *A39*, 377–387.

(89) Goldstein, S.; Ciupitoiu, A.; Vasilescu, V.; Duca, Al. *Mikrochim. Acta* **1975**, *I*, 117–123.

(90) Brown, K. L.; Satyanarayana, S. *Inorg. Chem.* **1992**, *31*, 1366–1369.

(91) Coppens, P. X-Ray Charge Densities and Chemical Bonding. *IUCR Texts on Crystallography*; Oxford University Press: Oxford, U.K., 1997.

(92) Madsen, A. Ø.; Sørensen, H. O.; Flensburg, C.; Stewart, R. F.; Larsen, S. *Acta Crystallogr.* **2004**, *A60*, 550–561.

(93) Overgaard, J.; Clausen, H. F.; Platts, J. A.; Iversen, B. B. *J. Am. Chem. Soc.* **2008**, *130*, 3834–3843.

(94) Frenking, G.; Fröhlich, N. *Chem. Rev.* **2000**, *100*, 717–774.

(95) Meister, J.; Schwarz, W. H. E. *J. Phys. Chem.* **1994**, *98*, 8245–8252.

(96) Bytheway, I.; Figgis, B. N.; Sobolev, A. N. *J. Chem. Soc., Dalton Trans.* **2001**, 3285–3294.

(97) Gatti, C.; Lasi, D. *Faraday Discuss.* **2007**, *135*, 55–78.

(98) Gatti, C.; Bertini, L. *Acta Crystallogr.* **2004**, *A60*, 438–449.

(99) Hübschle, C. B.; Luger, P. *J. Appl. Crystallogr.* **2006**, *39*, 901–904.

(100) Savin, A.; Nesper, R.; Wengert, S.; Fässler, T. F. *Angew. Chem.* **1997**, *109*, 1892–1918.

(101) Fässler, T. F.; Savin, A. *Chem. Unserer Zeit* **1997**, *3*, 110–120.

(102) Kohout, M.; Wagner, F. R.; Grin, Y. *Theor. Chem. Acc.* **2002**, *108*, 150–156.

(103) Kohout, M.; Savin, A. *Int. J. Quantum Chem.* **1996**, *60*, 875–882.

(104) Raub, S.; Jansen, G. *Theor. Chem. Acc.* **2001**, *106*, 223.

(105) Vidal, I.; Melchor, S.; Dobado, J. A. *J. Phys. Chem.* **2005**, *109*, 7500–7508.

JP902433X